Supporting information

Connectivity matters - Ultrafast isomerization dynamics of bisazobenzenes photoswitches

Chavdar Slavov,[a] Chong Yang,[b] Luca Schweighauser,[c] Chokri. Boumrifak,[a] Andreas Dreuw,[b] Hermann A. Wegner,[c,*] and Josef Wachtveitl[a,*]

[a] Institute of Physical and Theoretical Chemistry, Goethe University, Max-von-Laue-Str. 7, 60438 Frankfurt am Main, Germany.
[b] Theoretical and Computational Chemistry, Interdisciplinary Center for Scientific Computing (IWR), Im Neuenheimer Feld 368, 69120 Heidelberg, Germany.
[c] Institute of Organic Chemistry, Justus-Liebig University Giessen, Heinrich-Buff-Ring 17, 35392 Giessen, Germany.

We have investigated the ultrafast dynamics of *o*-, *m*- and *p*-bisazobenzenes, which represent elementary building blocks for photoswitchable multiazobenzene nanostructures. The connectivity pattern within bisazobenzenes and the ensuing complex interactions between the individual azobenzene units determines the ultrafast dynamics of these compounds and their photochemical properties. While retaining a relatively high E→Z isomerization quantum yield, *o*-bisazobenzene exhibits a very high thermal relaxation rate (half-life of 1.6 ms). Our theoretical calculations reveal that the geometry allows intramolecular excitonic interaction between the azobenzene units, which is reflected in the femtosecond transient absorption data via the simultaneous bleaching of the two excitonic bands. In contrast, the properties of *m*-bisazobenzene are very similar to the monomeric azobenzene, with the two units acting nearly independently from each other. The highest degree of π conjugation extending over the two azobenzene units was observed for *p*-bisazobenzene, which results in strong planarity of the molecule, reduced excited state lifetime and relatively low isomerization quantum yield. Multiphotochromic systems bridge the gap between molecular photoswitches and macroscopic function and thus, understanding the properties of bisazobenzenes opens the way to the design and development of new structures with extensive and versatile applications.

Experimental details

Sample preparation

General: All chemicals were used as purchased from the suppliers. NMR spectra were measured on Bruker Avance spectrometers (600 MHz or 400 MHz) at 298 K. Coupling constants (*J*) are reported in Hertz (Hz). The thermodynamically most stable *E*,*E*-isomer of each bisazobenzene is reported. EI-MS spectra were performed on a GC-MS HP 5890 with a HP 5971 mass detector. ESI-MS spectra were performed on a Bruker Micro TOF. Elemental analyses (EA) were measured on an Elementar Vario MICRO Cube. For preparative gel permeation chromatography (GPC) a Shimadzu Prominence recycling GPC was used. The separations were performed at room temperature with 2 x PSS linear S 600 x 20 mm columns (particle size 5 µm) by eluting with chloroform at a flow rate of 4 ml/min and continuous UV recording.

2-(Phenylazo)azobenzene: The 2-(phenylazo)azobenzene was synthesized according to literature.[1] ^{1}H-NMR (600 MHz, $CDCl_3$) δ 8.01 – 7.93 (m, 4H), 7.79 – 7.73 (m, 2H), 7.60 – 7.46 (m, 8H); ^{13}C-NMR (151 MHz, $CDCl_3$) δ 153.2, 148.3, 131.4, 131.0, 129.3, 123.4, 118.4; MS (EI) m/z (%) = 286 (37), 77 (100); HRMS (ESI) m/z $[M+Na]^+$ calc. for $C_{18}H_{14}N_4Na$: 309.1116; found: 309.1116; m.p. 109°C.

3-(Phenylazo)azobenzene:[2] Nitrosobenzene (1.14 g, 10.4 mmol, 1.20 eq.) was added to a solution of 3-nitroaniline (1.20 g, 8.63 mmol, 1.00 eq.) in 50 ml AcOH and was then stirred at rt overnight. The reaction mixture was concentrated under reduced pressure and the residue was purified by column chromatography (SiO_2, cyclohexane/ethyl acetate 50:1) to obtain the 3-nitroazobenzene as an orange solid (1.60 g). It was used without further purification for the next step. A solution of sodium hydrosulfide hydrate (1.09 g, 68%, 13.2 mmol) in 7 ml water was added to a solution of the crude 3-nitroazobenzene (1.00 g) in 35 ml ethanol. The reaction mixture was stirred for 1 h at rt. Then, 60 ml water were added to precipitate yellow crystals. The yellow solid was filtered off, washed with additional water and dried under vacuum to afford the crude 3-aminoazobenzene (588 mg). It was used without further purification for the next step. Nitrosobenzene (383 mg, 3.47 mmol) was added to a solution of the crude 3-aminoazobenzene (570 mg) in 15 ml AcOH. The reaction mixture was stirred over night at rt. Then, the solvent was removed under reduced pressure. The residue was purified by column chromatography (cyclohexane → cyclohexane/ethyl acetate 30:1), recrystallization form methanol and preparative GPC to isolate the pure product as a light orange solid (573 mg, 2.00 mmol, yield over three steps: 31%). ^{1}H-NMR (400 MHz, $CDCl_3$) δ 8.46 (t, *J* = 1.9 Hz, 1H), 8.06 (dd, *J* = 7.9, 1.9 Hz, 2H), 7.98 (dd, *J* = 8.2, 1.4 Hz, 4H), 7.68 (t, *J* = 7.9 Hz, 1H), 7.58 – 7.50 (m, 6H); ^{13}C-NMR (101 MHz, $CDCl_3$) δ 153.6, 152.7, 131.5, 129.8, 129.3, 125.5, 123.2, 116.6; MS (EI) m/z (%) = 286 (23) $[M]^+$, 77 (100); EA (%) calc. for $C_{18}H_{14}N_4$: C 75.50, H 4.93, N 19.57; found: C 75.38, H 5.01, N 19.85; m.p. 82°C. Analytical data corresponds to literature.[3]

4-(Phenylazo)azobenzene:[2,4] Nitrosobenzene (1.14 g, 10.4 mmol, 1.20 eq.) was added to a solution of 4-nitroaniline (1.20 g, 8.63 mmol, 1.00 eq.) in 50 ml AcOH and was then stirred at rt for 3 days. The reaction mixture was concentrated under reduced pressure and the residue was purified by column chromatography (SiO_2, cyclohexane/ethyl aceate 12:1) to obtain the 4-nitroazobenzene as a red solid (0.949 g). It was used without further purification for the next step. A solution of sodium hydrosulfide hydrate (0.956 g, 68%, 11.6 mmol) in 6 ml water was added to a solution of the crude 4-nitroazobenzene (0.878 g) in 31 ml ethanol. The reaction mixture was stirred for 3 h at rt. Then, 60 ml water were added to precipitate light orange crystals. The solid was filtered off, washed with additional water and dried under vacuum to afford the crude 4-aminoazobenzene (598 mg). It was used without further purification. Nitrosobenzene 4 (277 mg, 2.51 mmol) was added to a solution of crude 4-aminoazobenzene (412 mg) in 20 ml AcOH. The reaction mixture was stirred for 2 days at rt. Then, the solvent was removed under reduced pressure. The residue was purified by column chromatography (cyclohexane/ethyl acetate 50:1) and preparative GPC to isolate the pure product as a light orange solid (135 mg, 0.471 mmol, yield over three steps: 9%). ^{1}H-NMR (400 MHz, $CDCl_3$) δ 8.08 (s, 4H), 8.00 – 7.94 (m, 4H), 7.59 – 7.48 (m, 6H). ^{13}C-NMR (101 MHz, $CDCl_3$) δ 153.9, 152.9, 131.6, 129.3, 123.9, 123.2; MS (EI) m/z (%) = 286 (31) $[M]^+$, 77 (100); EA (%) calc. for $C_{18}H_{14}N_4$: C 75.50, H 4.93, N 19.57; found C 75.20, H 5.02, N 19.76; m.p. 170°C.

Steady-state spectroscopy and QY determination

A standard spectrophotomer (Specord S600, Analytik Jena) was used to measure the absorption spectra of the investigated compounds. The PSSs were generated as follows: i) PSS^{UV} was achieved by using a UV lamp (Hamamatsu L9588-01) combined with N-WG-320 and UG11 colour glass filters (SCHOTT) resulting in illumination at ~345 nm; ii) the PSS^{VIS} was achieved by using a 420 nm LED (ThorLabs M420L2). The QY of the $E \rightarrow Z$ isomerization after $\pi \rightarrow \pi^*$ excitation of the compounds was determined approximately by the grounds state bleach recovery in the transient absorption data.

Flashphotolysis experiments

The flashphotolysis measurements to determine the thermal $Z \rightarrow E$ back isomerization rate of the *o-bis*(AB) were performed on a home-built set-up based on a nanosecond Nd:YAG laser (1064 nm, Spitlight 600, Innolas Laser GmbH).[5] The third harmonic of the laser

was used for the pump pulses (~355 nm). The probe pulses were provided by a spectrally broad xenon flash lamp (2.9 µs pulses, LC-08, Hamamatsu). The detection system (~0.5 nm spectral resolution) was composed of a spectrograph (Acton SP2150, Princeton Instruments) and an ICCD camera (PIMAX 3, Princeton Instruments). The dataset was binned to a final wavelength resolution of ~4 nm.

Quantum chemical calculations

The absorption spectra of AB and the *bis*(AB)s structures have been calculated using time-dependent density functional theory (TD-DFT)[6-8] and algebraic diagrammatic construction scheme (ADC(2))[9-11]. TD-DFT is frequently used to calculate excited states and also has been proven successful in delivering accurate excitation energies for azobenzene.[12] In consideration of the computational efficiency and accuracy of the geometry and excited state calculations, ADC(2) was used to benchmark the results of TD-DFT calculations. To determine one suitable functional for an accurate description, the vertical excitation energies are evaluated at different theoretical levels (BLYP[13,14], BHLYP[15], B3LYP[16,17], TDHF[18-20] and ADC) with and without a conductor-like polarizable continuum model (C-PCM)[21-23] for ethanol solvation (dielectric constant of ε=24.5) (See Table S1 for comparison). Molecular ground-state geometries were optimized with DFT/BHLYP[15] using also the C-PCM for ethanol. Throughout all calculations the 6-31G* basis set[24] has been used. All calculations have been performed within Q-Chem 4.3.0 program.[25]

VIS-pump-probe spectroscopy

The femtosecond transient absorption set-up was described previously in detail.[26] In short it consists of an oscillator/amplifier system (Clark, MXR-CPA-iSeries, 775 nm, 150 fs, 1 kHz). The pump pulses between 300 and 430 nm (see text and figures for specific excitation wavelength) were generated by sum frequency mixing of pulses from a home-built two stage NOPA (non-collinear optical parametric amplifier)[27,28] and the laser fundamental. The pump pulse energy was adjusted to ensure that <10% of the molecules are excited per pulse. The probe pulse were generated by focusing the laser fundamental in a 5 mm thick CaF_2 crystal, which resulted in single filament white light (300-700 nm). The signal detection was done in reference mode by two spectrometers equipped with 600 lines/mm gratings, blazed at 300 nm.[26] The experiments were performed under magic angle conditions (54.7° pump-probe polarization angle difference) to eliminate anisotropic contributions. A prism compressor placed between the two NOPA stages was used to compress the NOPA pulses. The final pump-probe cross-correlation was ~100-130 fs. A fused silica cuvette with 1 mm optical path length was used for the experiments. The cuvette was continuously moved in the plane perpendicular to the direction of probe pulse propagation and illuminated (as described above) to maintain the PSS of interest.

Time-resolved data analysis

The time-resolved data were analysed by means of LDA, where the pre-exponential amplitudes in a sum of a large number (~100) of exponential functions with fixed, equally spaced (on a decimal logarithm scale) lifetimes are determined.[29] LDA is a model independent type of data analysis that naturally deals with non-exponential or stretched exponential kinetics. In this analysis, the lifetime distribution at each detection wavelength is obtained and thus the results can be presented in the form of a contour lifetime density map (LDM). A major advantage of the LDMs is that they can be used as kinetic footprint for a given sample under given conditions. In this respect, LDM are extremely useful in disentangling fine kinetic differences between similar samples/conditions. The coherent artifact contribution in the transient signals at time zero position was approximated with a function composed of a Gaussian and/or its first and second derivative[29,30] and fitted within the same routine as the LDA. The analysis was performed using OPTIMUS a data analysis program recently developed in our group.[29]

1. S. Bellotto, R. Reuter, C. Heinis and H. A. Wegner, *J. Org. Chem.*, 2011, **76**, 9826-9834.
2. H. Asanuma, X. G. Liang and M. Komiyama, *Tetrahedron Lett.*, 2000, **41**, 1055-1058.
3. P. Majumder, *et al.*, *Dalton Transactions*, 2011, **40**, 5423-5425.
4. K.-Y. Kim, J.-T. Shin, K.-S. Lee and C.-G. Cho, *Tetrahedron Lett.*, 2004, **45**, 117-120.
5. D. Chatterjee, *et al.*, *Angew. Chem. Int. Ed.*, 2015, **54**, 13555-13560.
6. E. Runge and E. K. U. Gross, *Phys. Rev. Lett.*, 1984, **52**, 997-1000.
7. M. E. Casida, *Recent Advances in Density Functional Methods*, World Scientific, 1995.
8. A. Dreuw and M. Head-Gordon, *Chem. Rev.*, 2005, **105**, 4009-4037.
9. J. Schirmer, *Phys. Rev. A*, 1982, **26**, 2395-2416.
10. M. Wormit, *et al.*, *Molecular Physics*, 2014, **112**, 774-784.
11. A. Dreuw and M. Wormit, *Wiley Interdisciplinary Reviews: Computational Molecular Science*, 2015, **5**, 82-95.
12. C. R. Crecca and A. E. Roitberg, *J. Phys. Chem. A*, 2006, **110**, 8188-8203.
13. A. Becke, *Phys. Rev. A*, 1988, **38**, 3098-3100.
14. C. Lee, W. Yang and R. Parr, *Phys. Rev. B*, 1988, **37**, 785-789.
15. A. D. Becke, *J. Chem. Phys.*, 1993, **98**, 1372-1377.
16. A. D. Becke, *J. Chem. Phys.*, 1993, **98**, 5648-5652.
17. P. J. Stephens, F. J. Devlin, C. F. Chabalowski and M. J. Frisch, *J. Phys. Chem.*, 1994, **98**, 11623-11627.
18. H. Sekino and R. J. Bartlett, *J. Chem. Phys.*, 1986, **85**, 976-989.
19. S. P. Karna, M. Dupuis, E. Perrin and P. N. Prasad, *J. Chem. Phys.*, 1990, **92**, 7418-7425.
20. S. P. Karna and M. Dupuis, *Journal of Computational Chemistry*, 1991, **12**, 487-504.
21. J. Liu and W. Liang, *J. Chem. Phys.*, 2011, **135**, 014113.
22. J. Liu and W. Liang, *J. Chem. Phys.*, 2011, **135**, 184111.
23. J. Liu and W. Liang, *J. Chem. Phys.*, 2013, **138**, 024101.
24. W. J. Hehre, R. Ditchfield and J. A. Pople, *J. Chem. Phys.*, 1972, **56**, 2257-2261.

25. Y. Shao*, et al.*, *Molecular Physics*, 2015, **113**, 184-215.
26. C. Slavov*, et al.*, *Phys. Chem. Chem. Phys.*, 2015, **17**, 14045-14053.
27. T. Wilhelm, J. Piel and E. Riedle, *Opt. Lett.*, 1997, **22**, 1494-1496.
28. E. Riedle*, et al.*, *Appl. Phys. B*, 2000, **71**, 457-465.
29. C. Slavov, H. Hartmann and J. Wachtveitl, *Anal. Chem.*, 2015, **87**, 2328-2336.
30. S. A. Kovalenko, A. L. Dobryakov, J. Ruthmann and N. P. Ernsting, *Phys. Rev. A*, 1999, **59**, 2369-2384.
31. J.-Å. Andersson, R. Petterson and L. Tegnér, *Journal of Photochemistry*, 1982, **20**, 17-32.

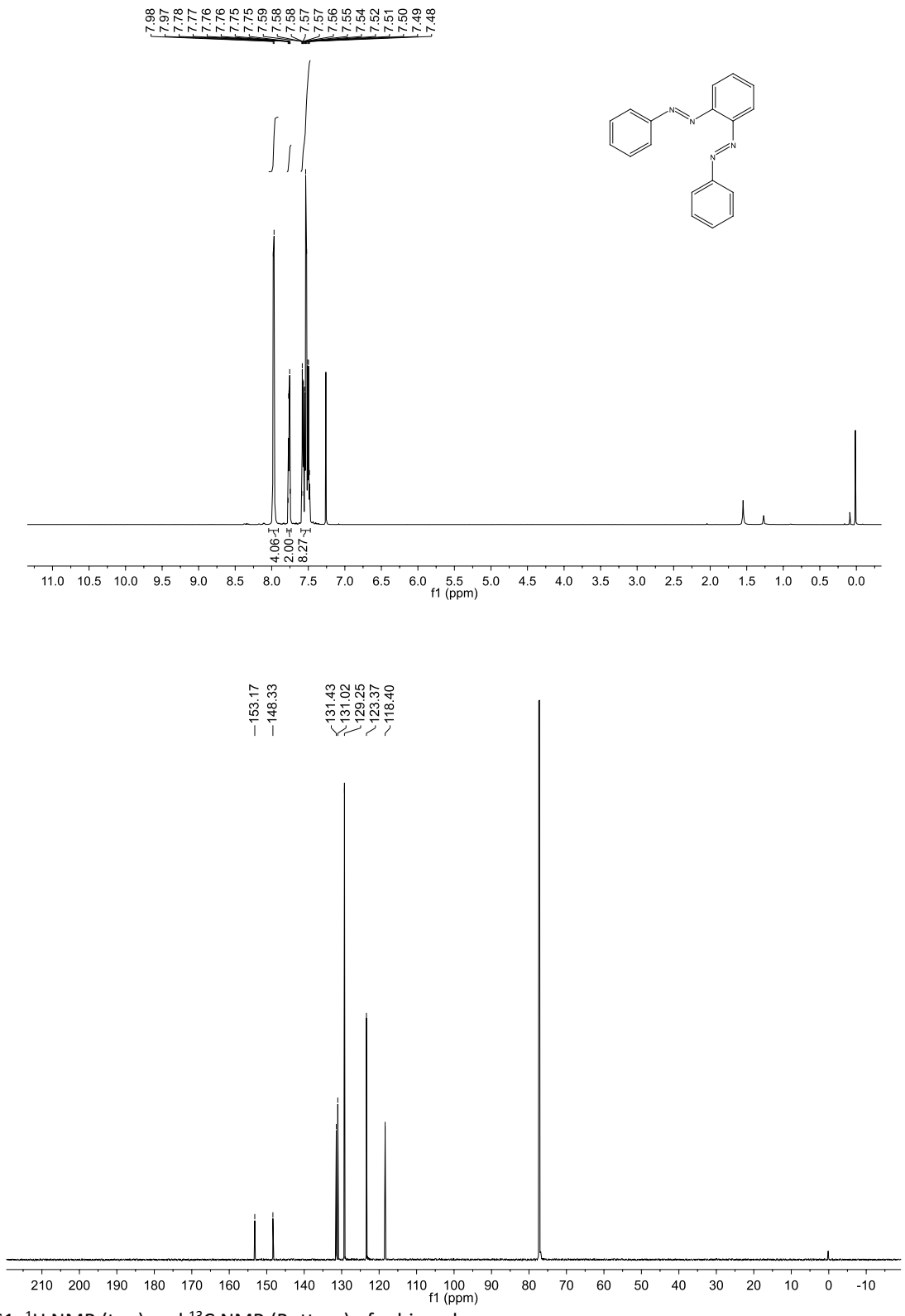

Fig. S1. ^{1}H NMR (top) and ^{13}C NMR (Bottom) of ***o***-bisazobenzene.

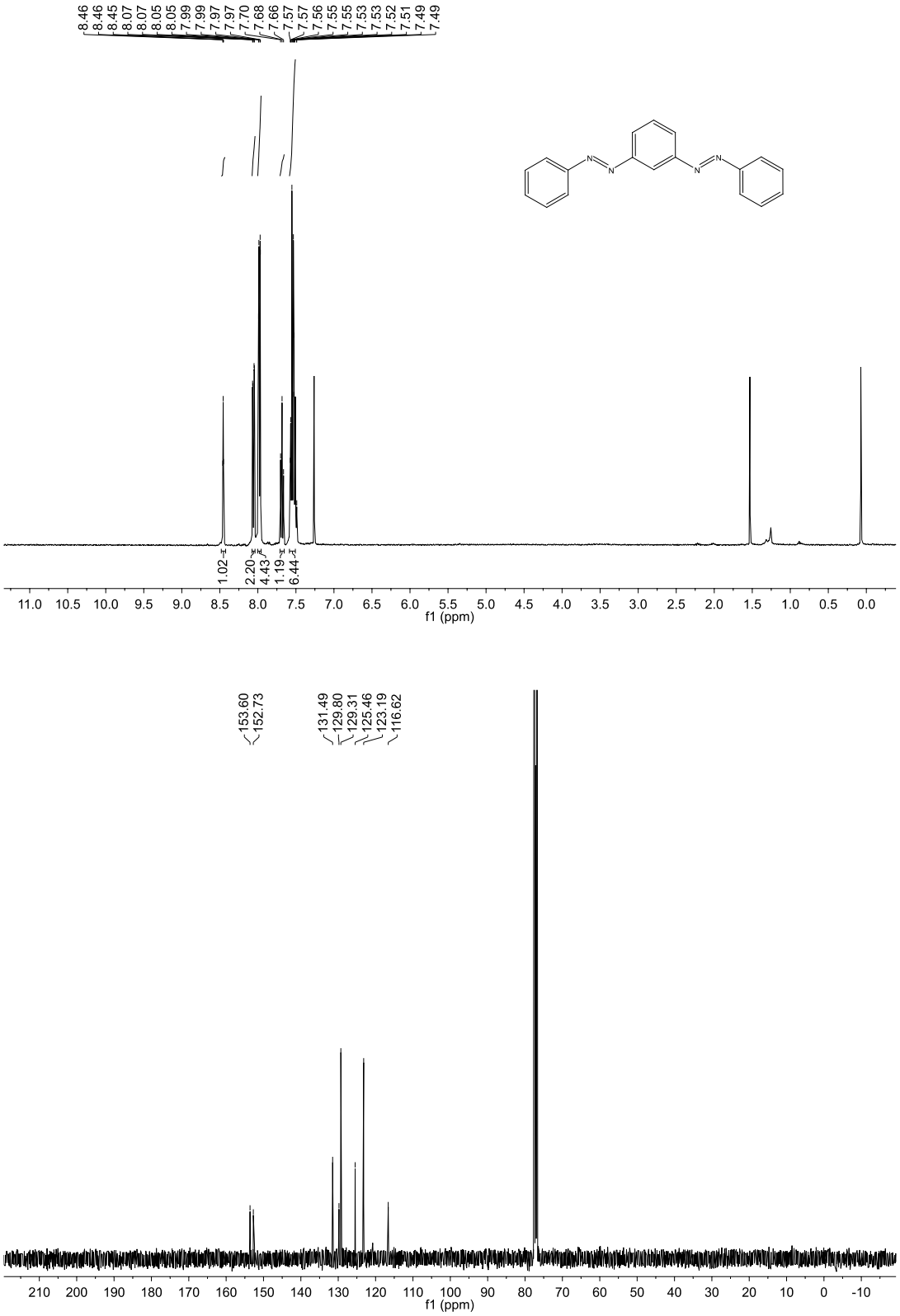

Fig. S2. ^{1}H NMR (top) and ^{13}C NMR (bottom) of ***m***-bisazobenzene.

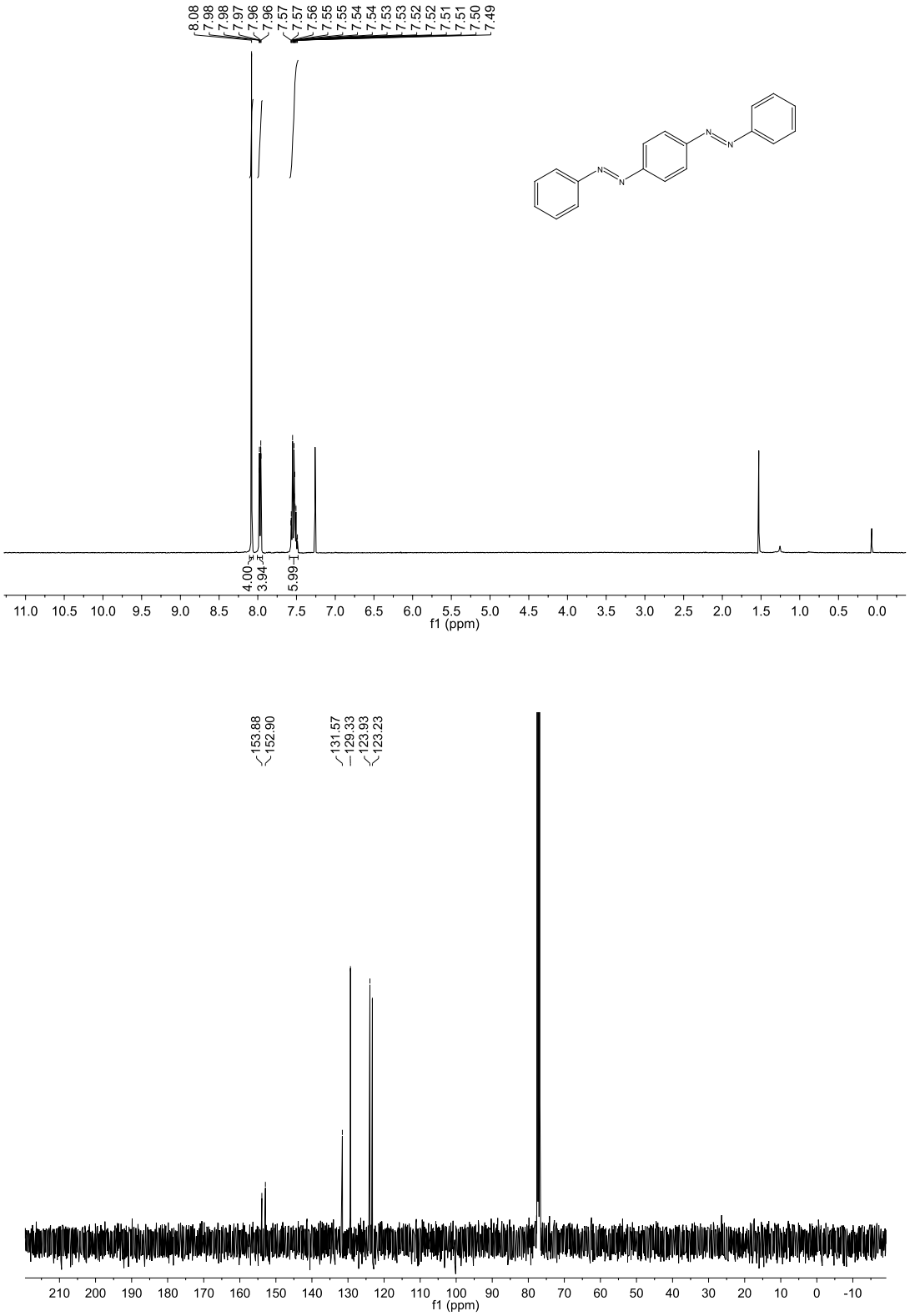

Fig. S3. ^{1}H NMR (top) and ^{13}C NMR (bottom) of ***p***-bisazobenzene.

Table S1. Comparison of the vertical excitation energies of the two low-lying excited states of E-AB using different approaches. The values are given in eV and in (nm).

***E*-AB**	***BLYP***		***B3LYP***		***BHLYP***		***TDHF***		***ADC(2)***		***EXPT.***	
	GAS	*C-PCM*	*GAS*	*C-PCM*	*GAS*	*C-PCM*	*GAS*	*C-PCM*	*GAS*	*C-PCM*	*GAS*	*solution*
S_1	2.2258 (557.03)	2.2866 (542.22)	2.5537 (485.85)	2.5946 (477.85)	2.9092 (426.18)	2.9314 (422.95)	3.2538 (381.44)	3.2585 (380.49)	2.99648 (413.77)	/	2.818[31] (440)	2.805* (442)
S_2	3.3573 (369.30)	3.1845 (389.34)	3.7717 (328.72)	3.5747 (346.84)	4.278 (289.82)	4.0910 (303.07)	4.8004 (258.28)	4.6450 (266.92)	4.34874 (285.10)	/	4.119[31] (301)	3.936* (315)

* taken from the experimental spectrum in Fig. 2 (ethanol).

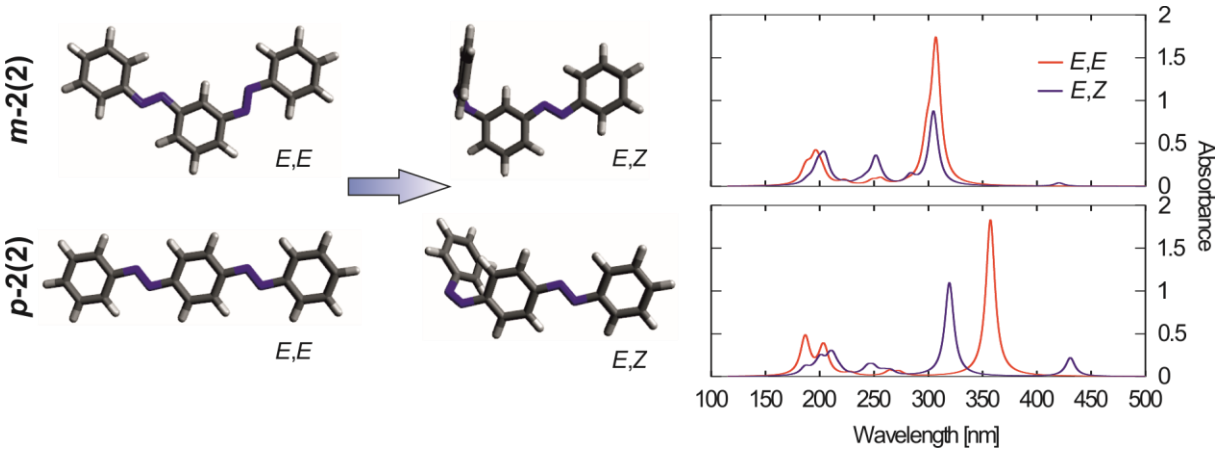

Fig. S5. Molecular structures of the additional *E*,*E* and *E*,*Z* isomers of ***m***- and ***p***-*bis*(AB) (left side) together with the corresponding simulated spectra using TDDFT/BHLYP/6-31G* with a PCM for ethanol (right).

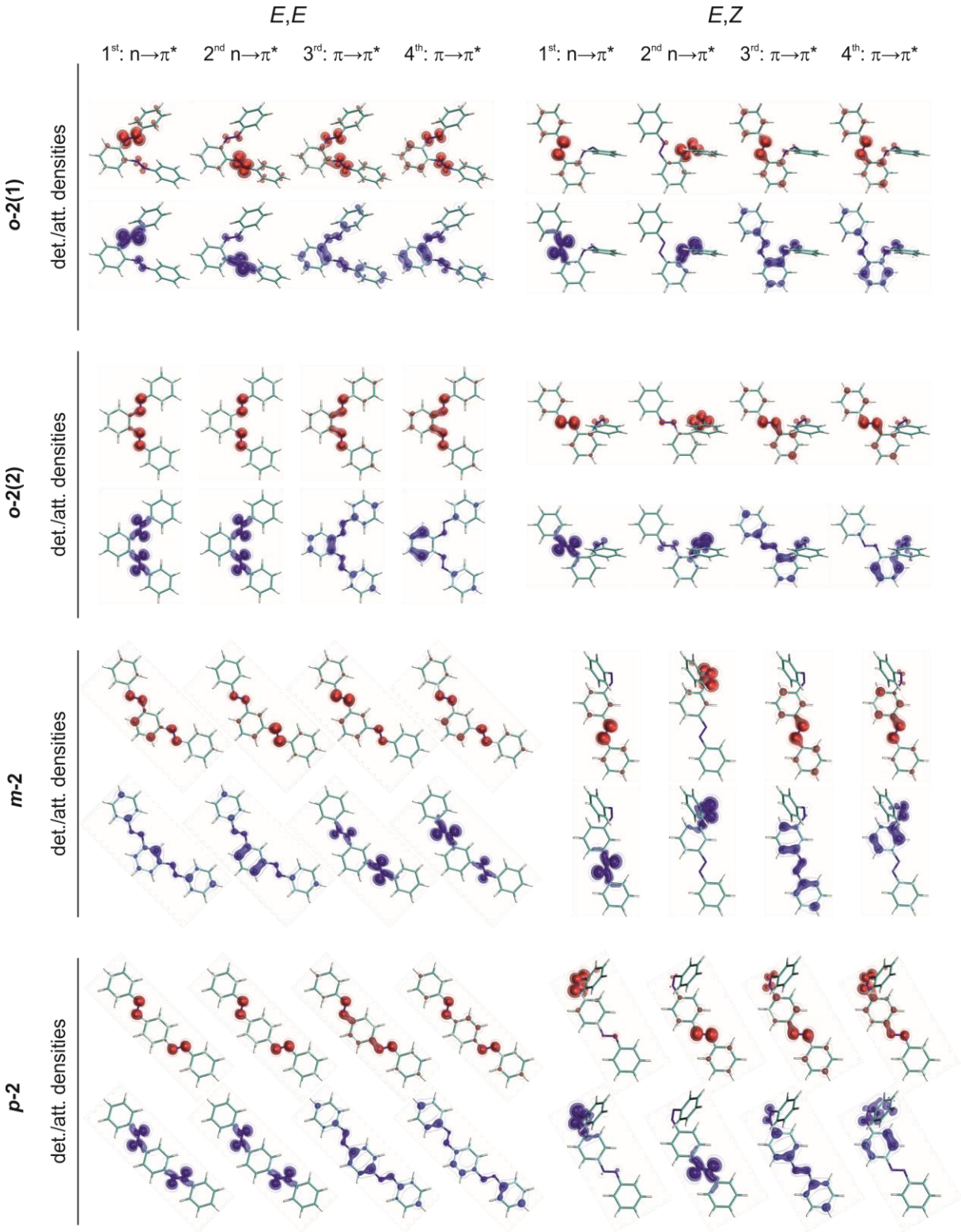

Fig. S5. Isosurfaces for attachment and detachment densities for the lowest excited states at the BHLYP/6-31G* level of theory for the investigated *bis*(AB) compounds.

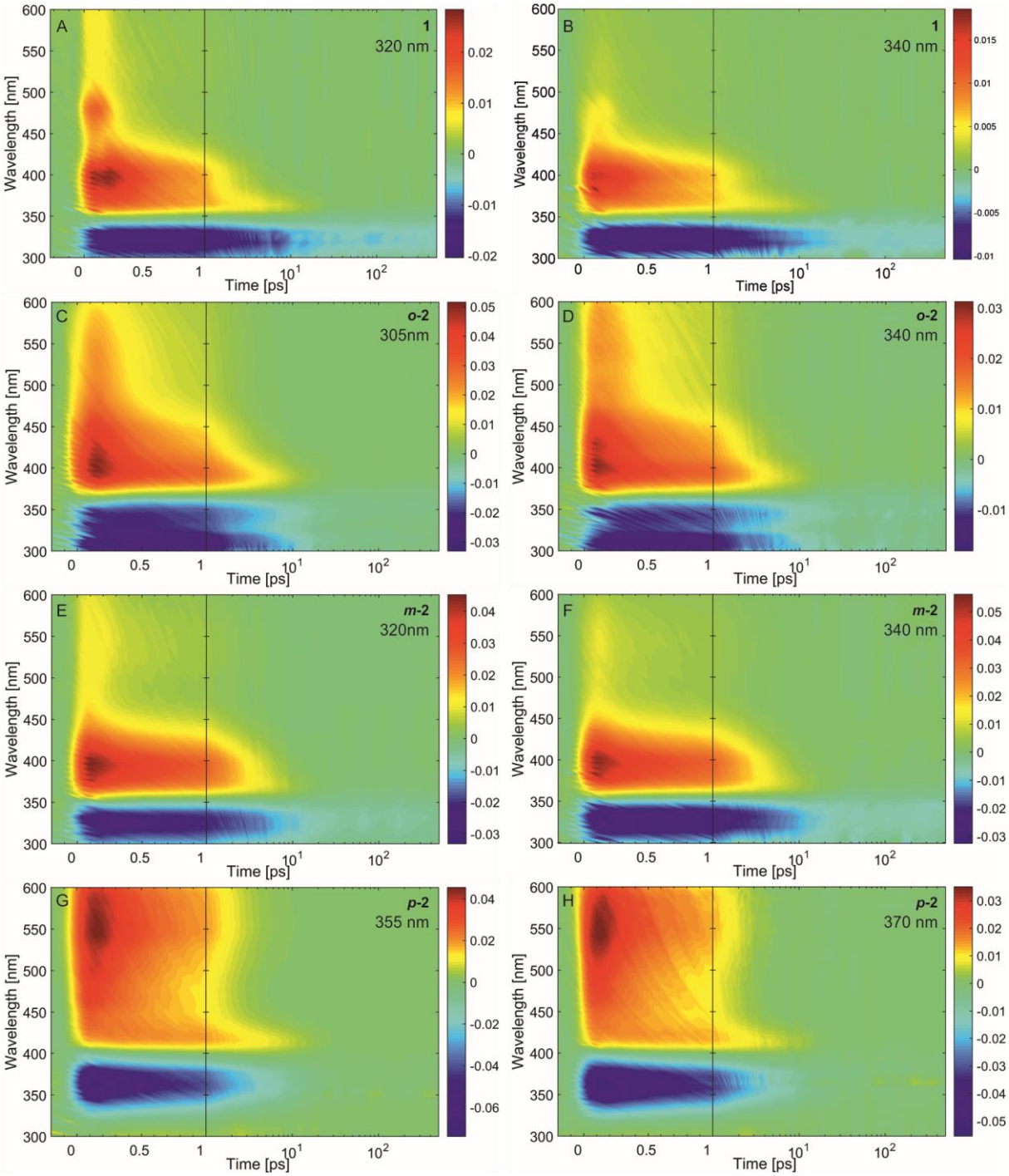

Fig. S6. Comparison of the femtosecond transient absorption data of the investigated compounds (as indicated) obtained after excitation in the maximum (A, C, E, G) of the *E*,*E*-isomer π→π* absorption band and in its red-shifted shoulder (B, D, F, H).

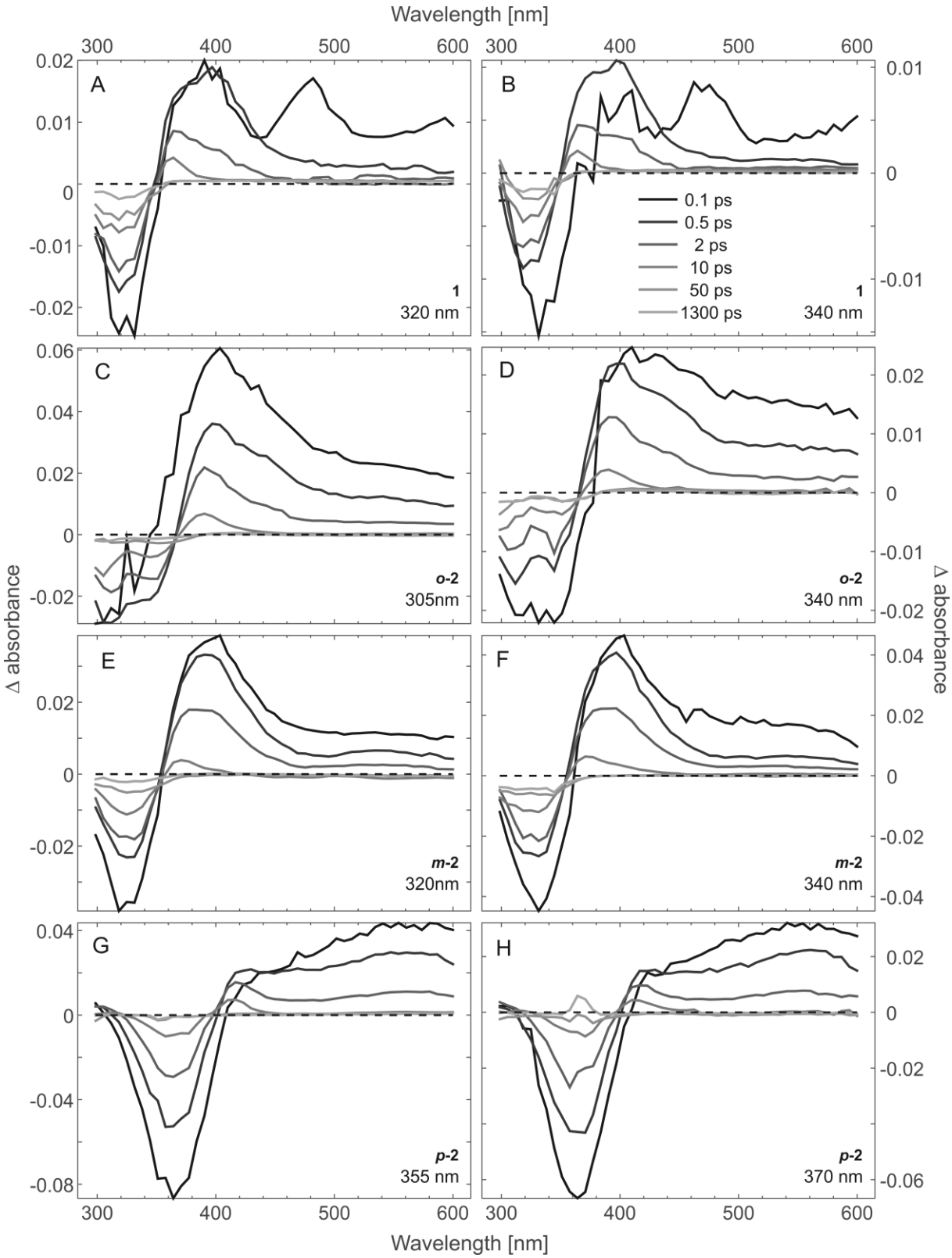

Fig. S7. Comparison of the transient absorption spectra of the investigated compounds (as indicated) obtained after excitation in the maximum (A, C, E, G) of the *E*,*E*-isomer π→π* absorption band and in its red-shifted shoulder (B, D, F, H).

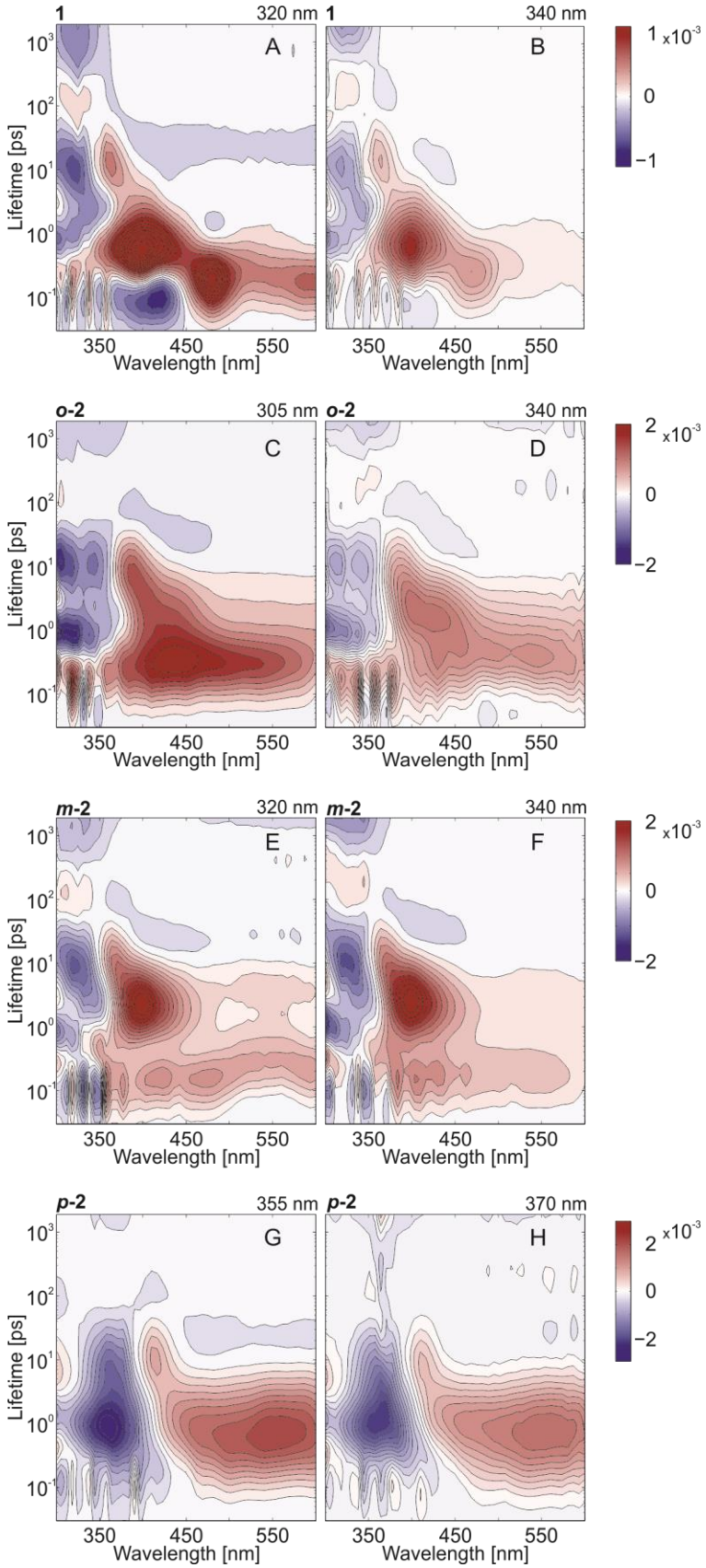

Fig. S8. Comparison of the . lifetime density maps reflecting the kinetics present in the transient absorption data of the investigated compounds (as indicated) after excitation in the maximum (A, C, E, G) of the *E*,*E*-isomer π→π* absorption band and in the its red-shifted shoulder (B, D, F, H). The negative-amplitude lifetime distributions at ~1 ns corresponds to the non-decaying component and thus to the final absorbance difference spectrum in the transient absorption data (Fig. S6 and S7).

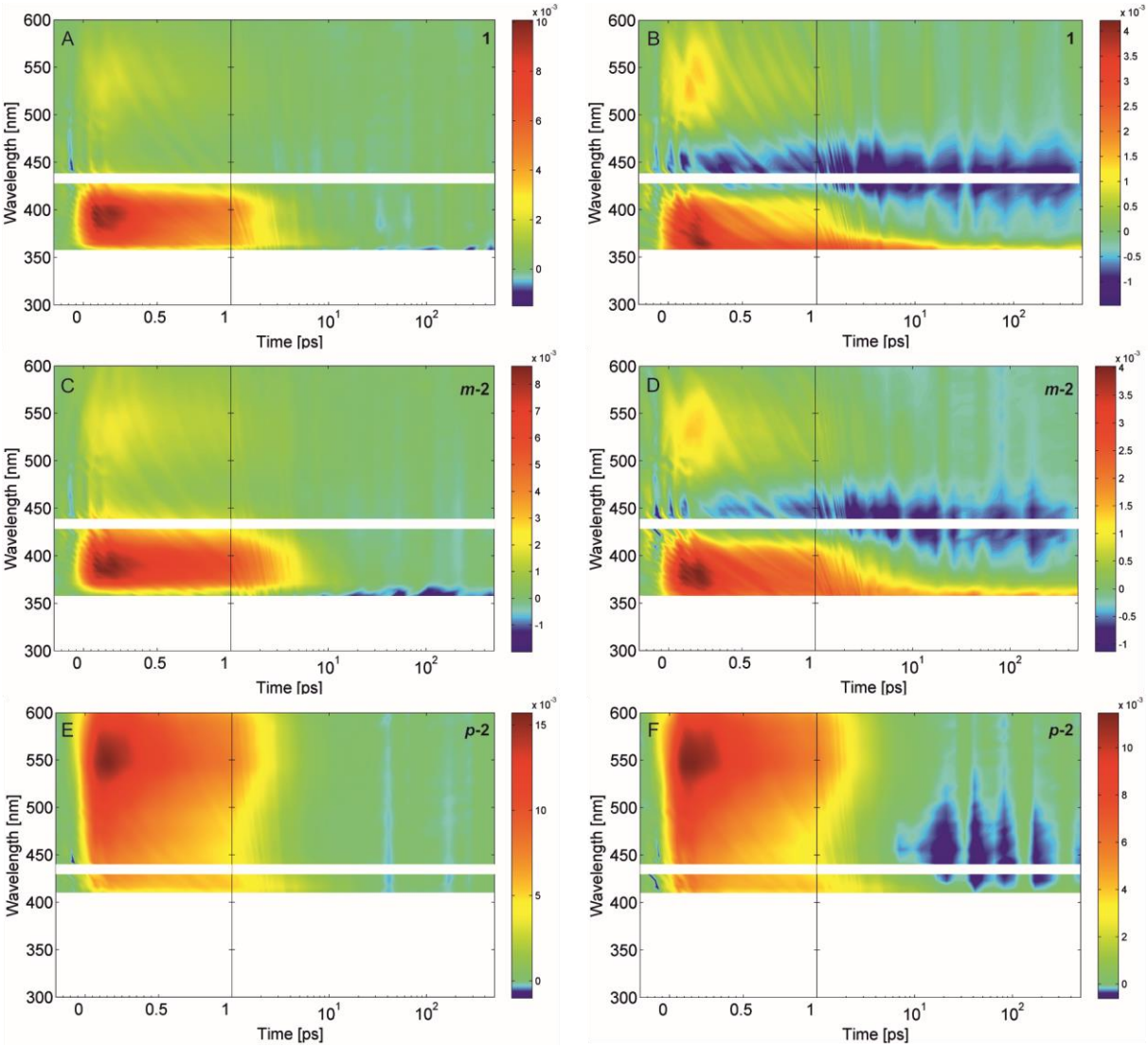

Fig. S9. Femtosecond transient absorption data of the investigated compounds (as indicated) obtained after excitation in the n→π* absorption band of the *E*,*E*-isomers (A, C, E) and of the *Z*-isomer (B, D, F).

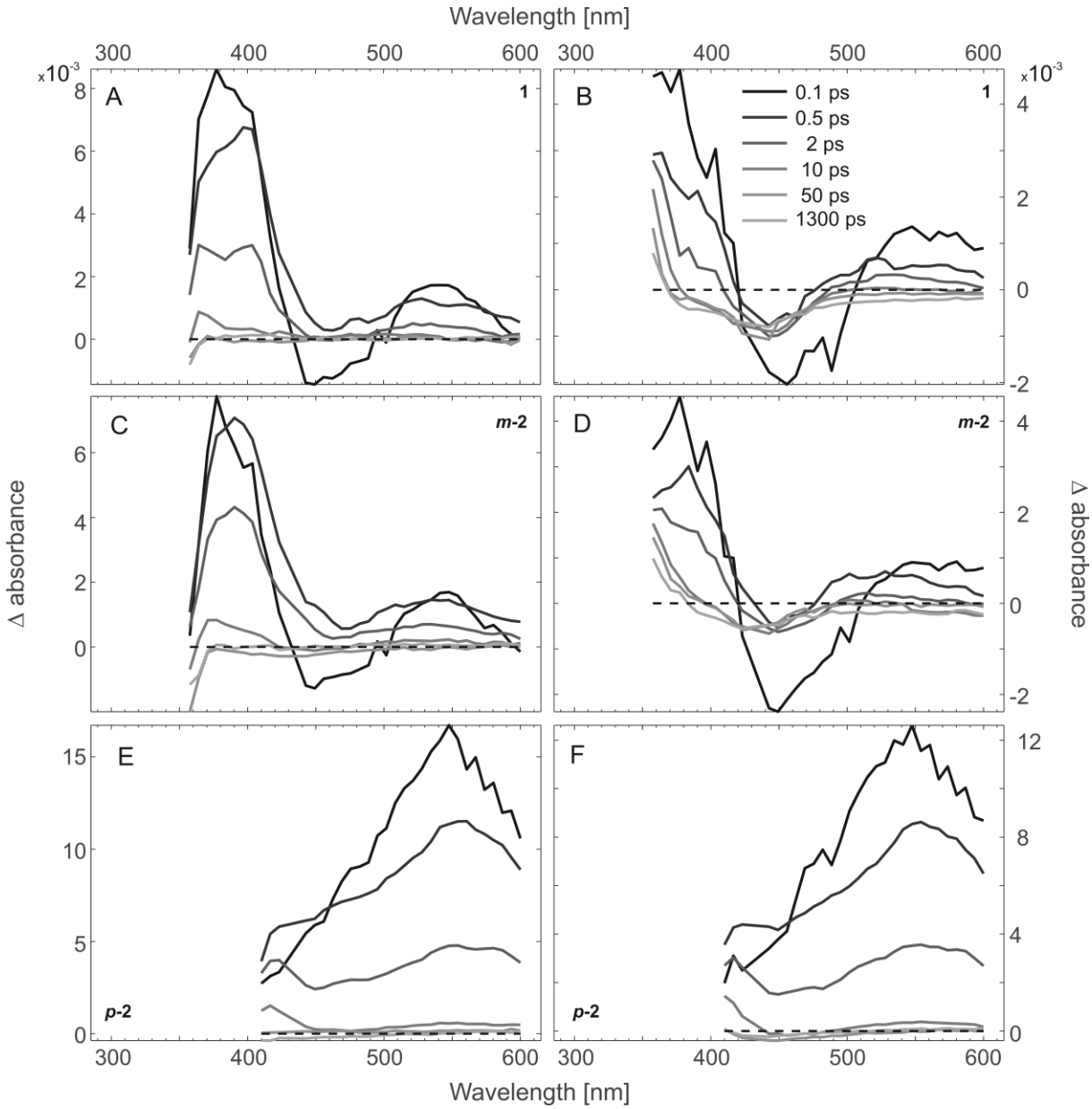

Fig. S10. Transient absorption spectra of the investigated compounds (as indicated) obtained after excitation in the n→π* absorption band of the *E*,*E*-isomer (A, C, E) and of the *Z*-isomer (B, D, F).

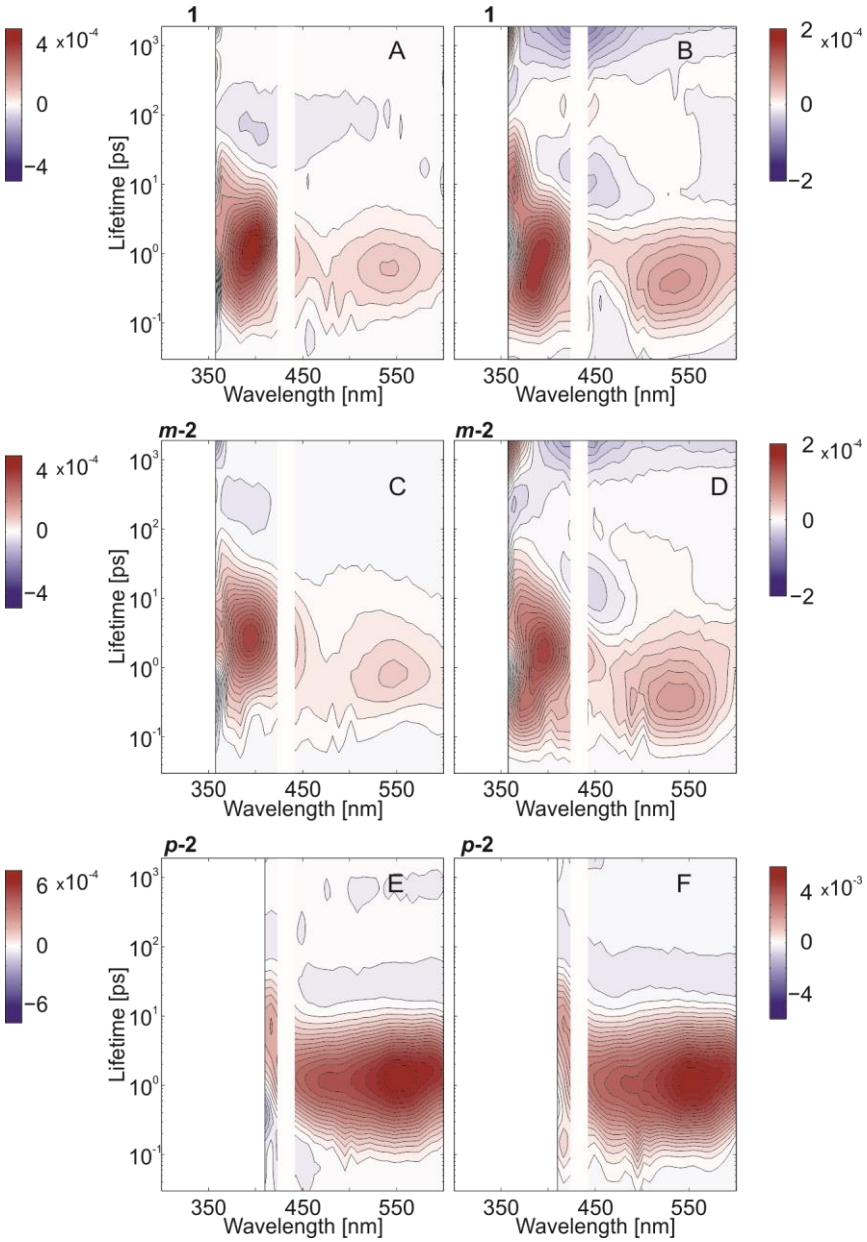

Fig. S11. Lifetime density maps reflecting the kinetics present in the transient absorption data of the investigated compounds (as indicated) after excitation in the n→π* absorption band of the *E*,*E*-isomer (A, C, E) and of the *Z*-isomer (B, D, F). The lifetime distributions at ~1 ns corresponds to the non-decaying component and thus to the final absorbance difference spectrum in the transient absorption data (Fig. S9 and S10).

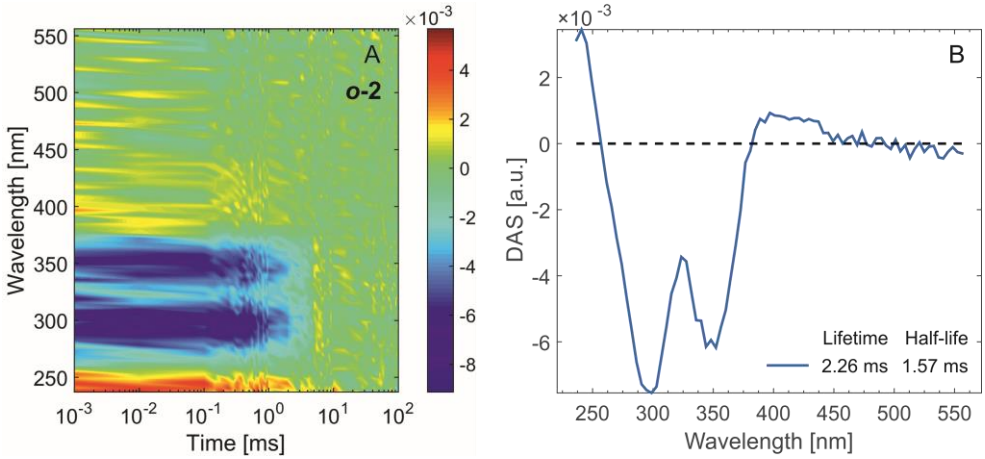

Fig. S12. A) Transient absorion data recorded after 355 nm excitation of the *E*,*E*-isomer of ***o*-2** using nanosecond flash photolysis. B) Global analysis of the transient absorption data in A). The lifetime of the *Z*-isomer is ~2.3 ms and thus the thermal *Z* → *E* isomerizaiton of ***o*-2** occurs with $t_{1/2}$ = 1.6 ms.

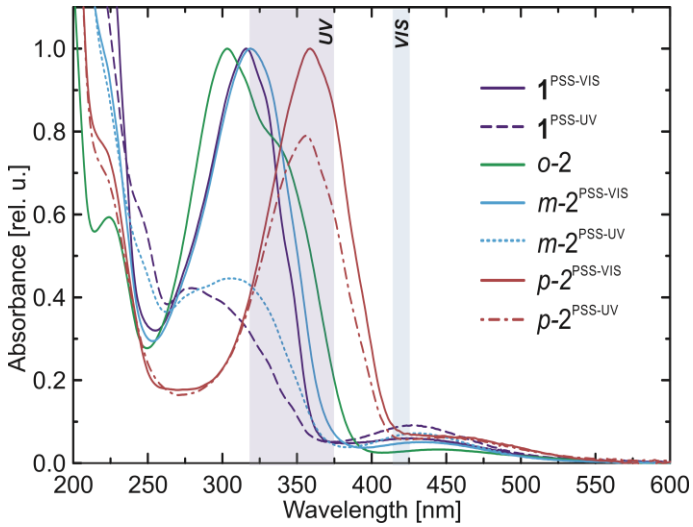

Fig. S13. Absorption spectra of the investigated compounds in the photostationary states (PSS) after VIS and UV irradiation. The transparent rectangulars (UV and VIS) mark the corresponding illumination wavelength ranges.